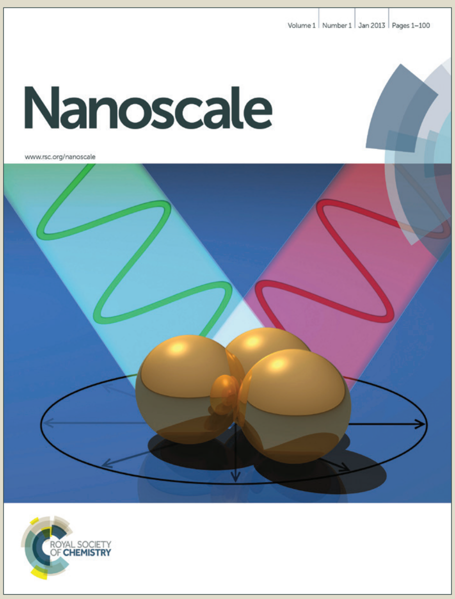

Volume 1 | Number 1 | Jan 2013 | Pages 1–100
Nanoscale
www.rsc.org/nanoscale
ROYAL SOCIETY OF CHEMISTRY

Graphical Abstract

Naturally aligned in-plane (without post-growth assembly), defect-free (without catalyst metal) and controllable GeSi nanowires are discovered via self-assembly of Ge on miscut Si (001) substrates by an angle θ (θ<11º) toward [100] direction.

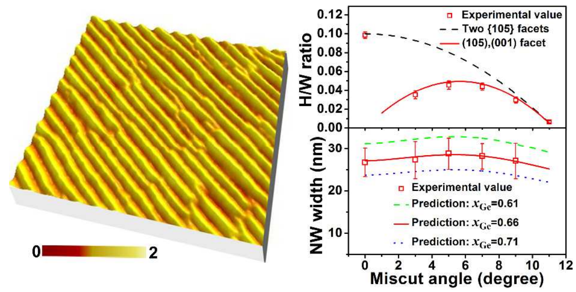

Cite this: DOI: 10.1039/c0xx00000x

www.rsc.org/xxxxxx

PAPER

Unique features of laterally aligned GeSi nanowires self-assembled on the vicinal Si (001) surface misoriented toward [100] direction

Tong Zhou,[a] Guglielmo Vastola,*[b] Yongwei Zhang,*[b] Qijun, Ren,[a] Yongliang Fan,[a] Zhenyang Zhong*[a]

Received (in XXX, XXX) Xth XXXXXXXXX 20XX, Accepted Xth XXXXXXXXX 20XX

DOI: 10.1039/b000000x

We demonstrate laterally aligned and catalyst-free GeSi nanowires (NWs) via self-assembly of Ge on miscut Si (001) substrates toward [100] direction by an angle θ (θ<11°). The NWs are bordered by (001) and (105) facets, which are thermodynamically stable. By tuning the miscut angle θ, the NW height can be easily modulated with the nearly constant width. The thickness of the wetting layer beneath the NWs also shows a peculiar behavior with a minimum at around 6°. An analytic model, considering the variation of both the surface energy and the strain energy of the epilayer on vicinal surfaces with the miscut angle and layer thickness, shows good overall agreement with the experimental results. It discloses that both the surface energy and the stain energy of the epilayer on vicinal surfaces can be considerably affected in the same trend by the surface steps. Our results not only shed new light to growth mechanism during heteroepitaxial growth, but also pave a prominent way to fabricate and meanwhile modulate laterally aligned and dislocation-free NWs.

1. Introduction

Semiconductor nanowires (NWs) are of special interest for their innovative application in quantum information processing,[1, 2] quantum transportation,[3] Josephson junction,[4] solar cells,[5] thanks to their unique properties.[6] To fully characterize and functionalize the semiconductor NWs, numerous strategies have been proposed to explore the controlled formation of NWs in aspects of size, shape, composition, orientation and arrangement.[7-9] The most common method for the formation of NWs is the so-called vapor-liquid-solid (VLS) method with the assistance of metal catalyst.[2, 4, 5, 7, 10] The obtained NWs have been broadly studied to explore the unique properties and the innovative device applications. On the other hand, it was found that the severe diffusion of the catalyst metal atoms into the NWs during growth was inevitable. Consequently, the properties of those NWs are degraded, and some of their applications are hampered by the contaminations and/or defects associated with the remained catalyst metal.[11] In addition, the obtained NWs are generally perpendicular to the substrate plane. Such out-of-plane NWs are not suitable for their general characterization and device applications, e.g. in the quantum transportation and the NW transistors without junctions,[3, 12] as well as subsequent integration of NW-based devices. Accordingly, various post-growth assembly methods have been developed for the horizontal incorporation of the out-of-plane NWs on the substrate surface.[13, 14] However, these methods still suffer from the complex production processes and low reproducibility, which restrict the mass-production of the fully aligned arrays of in-plane NWs. To circumvent these disadvantages, innovative approaches to the direct growth of in-plane NWs array without metal catalyst are highly desirable. Indeed, prototypical devices such as NW-based integrated circuits, and tunnel Field Effect Transistors, have recently been demonstrated based on horizontal NWs, although the growth of the NWs required substrate patterning or top-down approach.[15, 16] Therefore, studies on self-assembled, horizontal GeSi NWs on Si substrates become relevant for integration in nanodevices, because their monolithic integration could be simpler compared to vertically-grown NWs. For example, on a normal Si (001) surface, hut clusters can be elongated to become NWs during a thermal annealing.[17] On a vicinal Si (001) surface misoriented toward the <110> direction by several degrees, self-assembled GeSi nanostructures evolve from asymmetric-pyramid-like quantum dots (QDs) to NWs on the special case of Si (1 1 10) surface.[18-21] Whereas, in the former case, an extremely long annealing time is required. Moreover, the obtained GeSi NWs frequently intersect since the NWs can orient along either of the two perpendicular <100> directions. In the latter case, the formed GeSi NWs sensitively depend on the miscut angle. The issues of how to extend these criteria for the formation of NWs and how to readily control the NWs have not been clearly addressed. Despite the remarkable progress on the in-plane self-assembled NWs, it is still in the way to comprehensively learn the mechanism underlying the formation of NWs and find a feasible route to fabricate and manipulate the fully aligned in-plane and defect-free NWs.

In this letter, we report on the systematic studies on the self-assembly of Ge on the vicinal Si (001) surface misoriented toward [100] direction. It is found that the laterally aligned and defect-free GeSi NWs can be readily obtained on the vicinal surfaces with a considerably large range of misorientation anlges θ (θ<11°). The self-assembled GeSi NWs all oriented perpendicularly to the miscut direction and are stable against the thermal annealing and the high growth temperature. Furthermore, the height of the obtained GeSi NWs can be readily tuned by the miscut angle since the NWs are bordered by (001) and (105) facets and have nearly constant width. The thickness of the wetting-layer (WL) can be also tuned by altering the surface orientations and shows a non-uniform behavior with a minimum at around 6º miscut angle. To interpret these unique and fascinating features of self-assembled GeSi NWs on the vicinal Si (001) surface, a thermodynamic model based on Asaro-Tiller-Grinfelg (ATG) instability is proposed, which takes into account the misorientation-dependent surface energy and the interplay between the surface energy cost and the elastic strain relaxation of the NWs. The model exhibits very good agreement with the experimental results. Our results not only offer the insights into the nature of the heteroepitaxial growth on the vicinal substrates, but also demonstrate a promising route to both fabricate and tailor the laterally aligned and dislocation-free NWs for the characterization of their unique properties and innovative device applications.

2. Experiments

The samples were grown on vicinal Si (001) substrates with miscut angles θ toward [100] direction, which were denoted by Si (001)/[100] θ. All samples were grown by molecular beam epitaxy (MBE) in a Riber Eva-32. The substrates were cleaned using the RCA method, followed by a subsequent HF treatment to form hydrogen-terminated surface before loading into the growth chamber. After the thermal desorption at 840 ºC for 3 min, a Si buffer layer of 100 nm was grown at a growth rate of 0.6 Å/s while ramping the temperature from 500 ºC to 580 ºC to obtain smooth surface without kinetic step-bunching. Subsequently, Ge was deposited at different temperatures from 515 ºC to 650 ºC at a growth rate of 0.05 Å/s. For the annealing sample on Si (001)/[100] 7º, an in-situ annealing process at 540 ºC for about two hours after Ge deposition was carried out. The surface morphologies of the samples were characterized using atomic force microcopy (AFM) (Veeco DI Multimode V SPM) in tapping mode.

3. Results and Discussions

Figures 1(a) and 1(b) show the surface morphologies after 6 and 5.4 monolayers (ML) Ge deposition at 540 ºC on Si (001)/[100] 0º and Si (001)/[100] 7º, respectively. Elongated Ge QDs, referred to as 'hut clusters' with {105} facets,[22] are randomly distributed on the Si (001)/[100] 0º substrate. Interestingly, on the Si (001)/[100] 7º substrate, the laterally aligned GeSi NWs appear, which are compactly arranged and show well uniformed lateral width. We find that all NWs orient along [010] direction that is perpendicular to the miscut direction of [100]. These self-assembled NWs are remarkably different from previously reported ones.[17, 18, 20] The GeSi NWs, obtained after extremely long annealing time on the normal Si (001) substrates, orient along either of two perpendicular <100> directions and intersect frequently.[17] On vicinal Si (001) substrates with ~8º off towards [110] direction, the obtained GeSi NWs all nearly orient parallel to the miscut direction of [110].[18, 20] Furthermore, such small and compactly arranged Ge-rich NWs

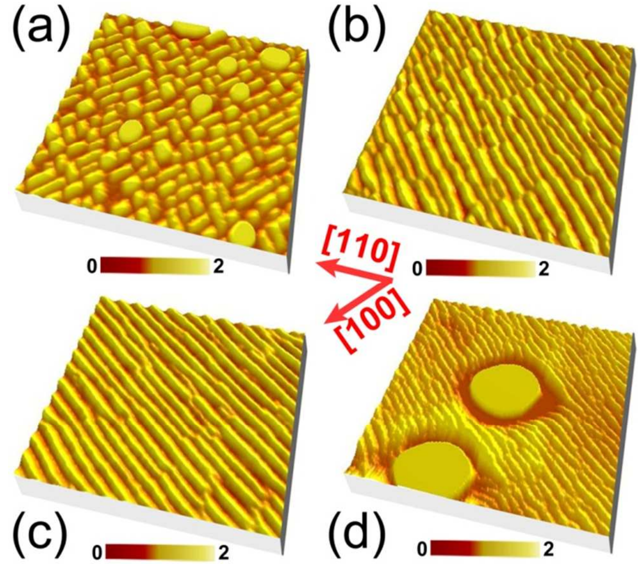

Fig. 1 AFM images ($0.5\times0.5\mu m^2$) of the surface morphologies, (a) 6 ML Ge deposition at 540 ºC on Si (001)/[100] 0º; (b) 5.4 ML Ge deposition at 540 ºC on Si (001)/[100]7º; (c) 5.4 ML Ge deposition at 540 ºC with a subsequent in-situ annealing for two hours on Si (001)/[100] 7º; (d) 5.4 ML Ge deposition at 650 ºC on Si (001)/[100] 7º. The unit of color bar is nm.

are rather stable. Fig. 1(c) shows the surface morphology after 5.4 ML Ge deposition at 540 ºC on Si (001)/[100] 7º and a subsequent in-situ annealing for two hours. The NWs remain after the annealing. By comparing the NWs in Figs. 1(b) and 1(c), we find that the most pronounced effect of the annealing results in the better uniformity and the longer of the NWs. This result indicates that the self-assembled NWs can be improved by proper annealing processes. Fig. 1(d) shows the surface morphology after 5.4 ML Ge deposition at 650 ºC on Si (001)/[100] 7º. It can be seen that large domes and compactly arranged NWs coexist. Essentially no denuded zone appears around the large domes. These results demonstrate that the NWs are rather stable and the Ostwald ripening of the NWs can be effectively suppressed on the vicinal surface. This is considerably different from the case on a normal Si (001) substrate.[23] By comparing the NWs grown at different temperatures, we discover that the width of the NWs tends to decrease with the increase of the growth temperatures, as shown in Figs. 1 (b) and (d). This result is completely distinguishable from the previous ones related to the step-bunching.[24] Meanwhile, the step-bunching always results in GeSi ripples with a width ranging from 100 nm to more than 1 μm, which are much larger than the NWs observed here.[25-28]

Figures 2(a)-2(f) show the surface morphologies after 5.4 ML Ge deposition at 515 ºC on Si (001)/[100] θ (θ=0º, 3º, 5º, 7º, 9º, and 11º). Apparently, the surface morphologies considerably depend on the substrate orientations. On the normal Si (001) substrate, hut clusters appear, as shown in Fig. 2(a). On the Si (001)/[100] θ (θ=3º, 5º, 7º, and 9º) substrates, laterally aligned NWs are evident, as shown in Fig. 2 (b)-(d). In the case of the miscut angle of 11º, the vicinal surface is still quite flat after Ge deposition, which in fact approaches to the (105) facet. Accordingly, the formation of nanostructures (e.g. hut-cluster, pyramid and NWs) bordered by {105} facets is essentially

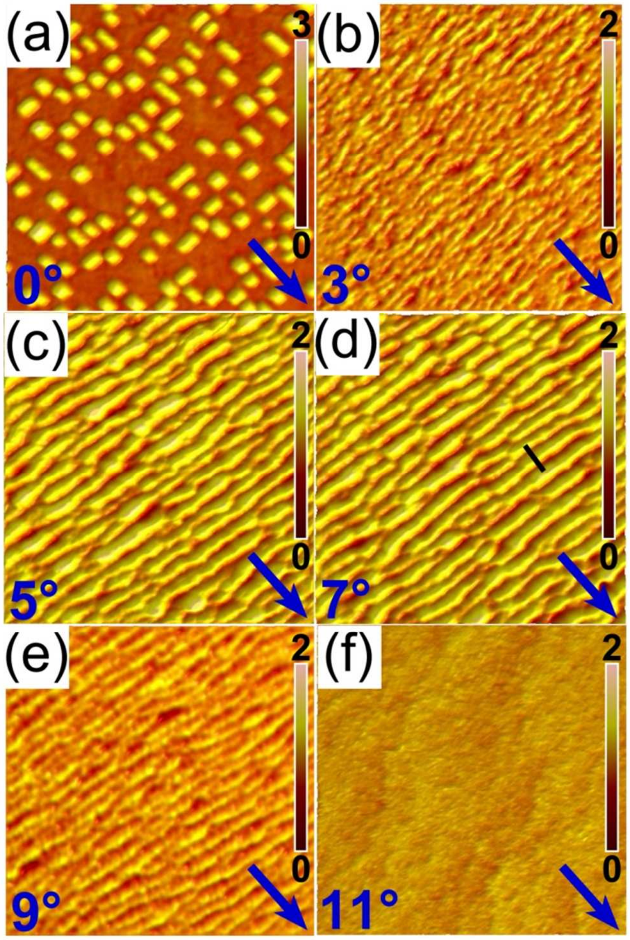

Fig. 2 AFM images ($0.5\times0.5\mu m^2$) of the surface morphologies after 5.4 ML Ge deposition at 515 ºC on Si (001) /[100] θ with, (a) θ=0º, (b) θ=3º, (c) θ=5º, (d) θ=7º, (e) θ=9º, (f) θ=11º, respectively. The miscut direction of [100] is denoted by the arrow. The unit of color bar is nm.

suppressed. Only few dome-like islands appear in a large area since their critical volume and energy barrier are both quite large. Interestingly, we find that the orientation of NWs is independent on the miscut angle and all along the [010] direction. Whereas, the sizes of NWs are considerably affected by the miscut angle. These results demonstrate that the laterally aligned GeSi NWs are readily self-assembled on the vicinal Si (001)/[100] θ (θ<11º) substrates. Moreover, the geometries of the NWs can be tuned by the miscut angle.

To obtain the actual geometries of NWs, we firstly analyze the cross-sectional height profile of the NWs, as shown in Fig. 3(a). It clearly exhibits the width and the height of the NWs to be about 25nm and 1nm, respectively. Moreover, an asymmetry is observed. Based on the profile, we can extract the intersection angles between the two sidewalls of the NWs and the vicinal surface to be about 4º and 7º, as denoted in Fig. 3(a). On the Si (001)/[100] 7º substrates, the intersection angle between (105) and (-105) facet and the vicinal surface is about 4º and 18º, respectively. The angle between (001) facet and the vicinal surface is 7º. These results suggest that the NWs on the Si (001)/[100] 7º substrates are bordered by (001) and (105) facet rather than the two {105} facets ((105) and (-105)).[18, 20] In order to clarify whether the NWs on the other Si (001)/[100] θ

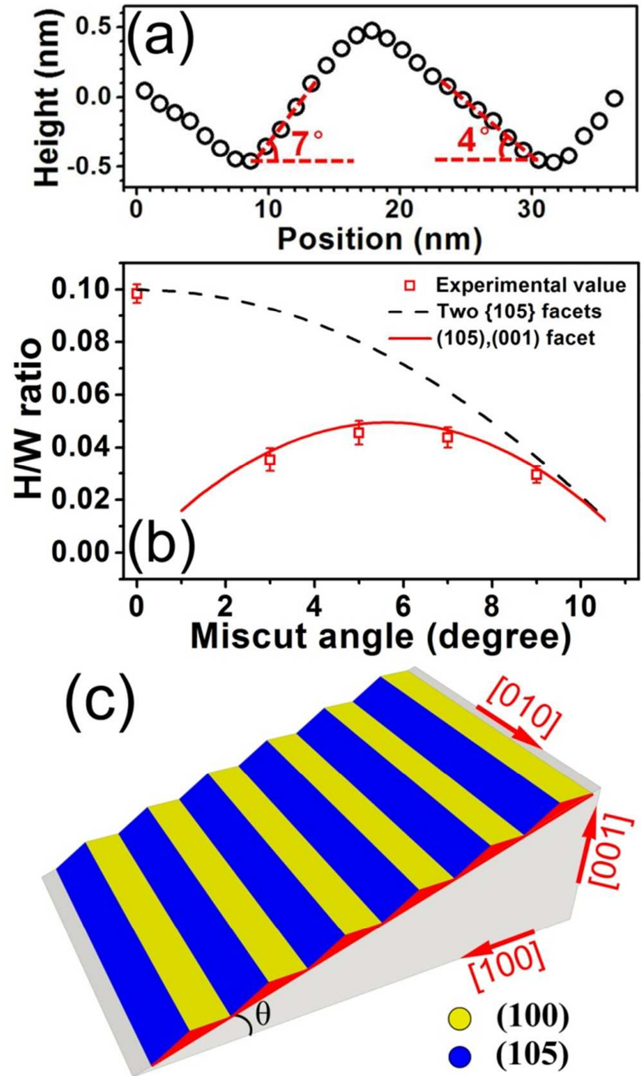

Fig. 3 (a) The cross-sectional height profile of the NWs along the line in Fig. 2(d); (b) the aspect ratio between the height (H) and the width (W) of the NWs (in Fig. 2) as a function of the miscut angles. The scattered points represent the experimental values derived from the AFM images. The solid and dashed lines represent the ideal aspect ratio for the NWs bordered by ((105) and (001) facets) and ((105) and (-105) facets), respectively; (c) The Schematic illustration of the NWs on the Si (001)/[100] θ substrate.

substrates are also bordered by (001) and (105) facets, we extracted the aspect ratio between the height and the width of the NWs in Figs. 2 as a function of the miscut angles, as shown in Fig. 3(b). The aspect ratios corresponding to the NWs bordered by two {105} facets and by (001) and (105) facets are calculated and also shown in Fig. 3(b). The experimental aspect ratios of the NWs are well fitted by the theoretical ones corresponding to the border of (001) and (105) facets. Based on the results in Figs. 3(a) and 3(b), we argue that the NWs on vicinal Si (001)/[100] θ substrates are essentially bordered by (001) and (105) facets, as schematically shown in Fig. 3(c).

To further study the impacts of the miscut angle on the self assembly of the NWs on the vicinal surface, we investigate the NW width as a function of the miscut angle, as shown in Fig. 4. Surprisingly, the NW width is nearly not affected by the miscut angle, which is about 27nm on all vicinal surfaces in our cases.

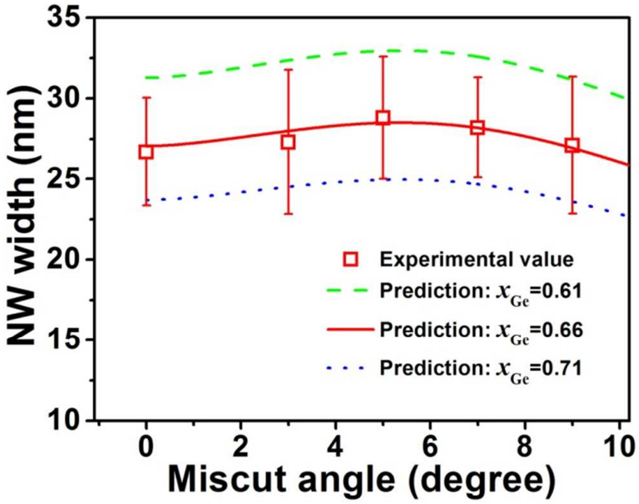

Fig. 4 The NW width vs the miscut angle. Calculations are shown for three representative $Si_{1-x}Ge_x$ compositions of x=0.61 (dashed line), 0.66 (solid line) and 0.71 (dotted line).

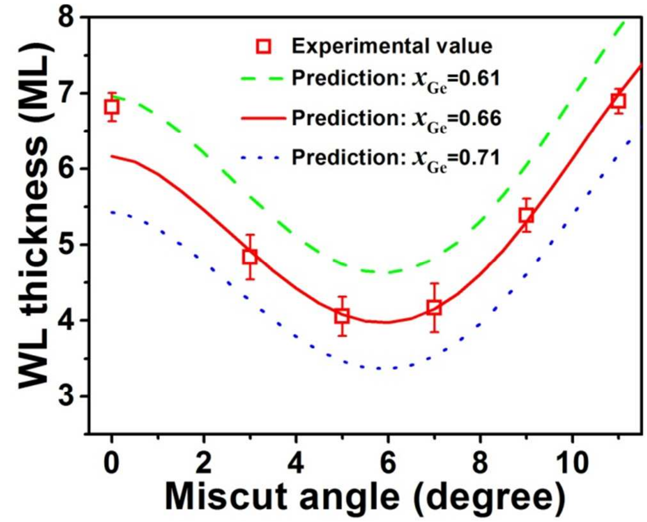

Fig. 5 The wetting-layer (WL) thickness vs the miscut angle. Calculations are shown for three representative $Si_{1-x}Ge_x$ compositions of x=0.61 (dashed line), 0.66 (solid line) and 0.71 (dotted line).

Considering the aspect ratios in Fig. 3(b), we find that the height of the NWs can be readily tuned by the miscut angle of the vicinal surface. This result indicates that the miscut angle offers a promising degree to modulate the properties of the NWs. This peculiarity can become important when tailoring the functionalities of devices based on the NWs. In addition, the overall volume of the NWs on the vicinal surface considerably depends on the miscut angle. Accordingly, the thickness of the WL below the NWs is affected by the miscut angle. The NWs Ge composition was measured by Raman spectra. The measurements show a Ge content of 66%. Notably, we did not find a significant variation of Ge composition with miscut angle. Details of the Raman measurements are reported in Supplementary Data (see, for example, Figure S1). The value of 66% Ge composition was used as input for our modeling calculations. Further, the calculations were repeated for the Ge contents of 61% and 71% to account for the uncertainty in the Raman measure. Given the total amount of deposited Ge and the Ge composition in NWs, we can extract the WL thickness on different miscut substrates. The WL thickness as a function of the misuct angle is shown in Fig. 5. It is revealed that the thickness of the WL show a non-monotonic behavior. A minimum value exists for the miscut angle of ~6º. These findings suggest that the onset of the 2D-to-3D growth transition can be tuned by the modification of substrate orientation.

In order to gain insights into the nature of self-assembled GeSi NWs on miscut Si (001) substrate, analytical modeling of the heteroepitaxial growth is performed. We carry out a quantitative explanation for the behaviors of the Ge NWs on the vicinal surface with the focus on the initial stages of the NW nucleation. Therefore, a linear stability analysis is used, as first introduced by Asaro and Tiller and by Srolovitz.[29, 30] We begin by modeling the GeSi surface energy as a function of the miscut angle θ,[31] as shown in the following,

$$\gamma(\theta,h)=\gamma_0(h)+a(h)\tan^2\theta+b(h)\tan^3\theta+c(h)\tan^4\theta \qquad (1)$$

where the parameters $a(h)$, $b(h)$, $c(h)$ account for the dependence on the thickness of thin film and $\gamma_0(h)$ is the surface energy of a zero-miscut film of thickness h. Such dependence of surface energy on the film thickness has been well-documented in literature.[28, 32-34] For example, a linear term is absent in Eq.(1) to give a smooth derivative for γ as θ→0, necessary to reproduce early experiments of GeSi growth on Si(001).[31] Overall, Eq.(1) correctly captures the key features of the Ge surface energy with misorientation, namely, a local maximum around 6° as well as the well-know minimum at 11.4°.[35, 36] In particular, the parameters are fitted to reproduce the *ab-initio* results for the (001) and (105) Ge stable facets, where surface reconstruction is taken into account.[37] As a result, our surface energy locally reproduces the values computed at specific surface inclination, and Ge film thickness.[20] Therefore, our parameters are indeed those required to reproduce existing literature data and details on their derivation are reported in the Supplementary Data.[37] The dependence of the surface energy on the miscut angle θ and the thickness h is depicted in Figure 6, according to Eq. (1). In attachment-detachment kinetics during the heteroepitaxial growth, surface undulations can spontaneously arise because of the in-plane stress in thin film. The fastest-growing undulation wavelength λ is given by,[30]

$$\lambda=\frac{3}{4}\frac{\pi}{2}\frac{\gamma}{w} \qquad (2)$$

where w is the thin film elastic energy density. Evaluation of w is carried out considering the anisotropy of elastic constants for both Ge and Si.[38, 39] Intermixing between Ge and Si is included by considering an average $Si_{1-x}Ge_x$ composition.[40] The Youngs's modulus and Poisson ratio of the alloy is calculated according to Vegard's law. The fastest-growing undulation evaluated from the Eq. (2) as a function of miscut angle is shown in Fig. 4 for three different average Ge compositions, namely 0.61, 0.66 and 0.71. The Figure shows that the model predictions and the measured surface wavelength are in good agreement. Based on Eq. (2), the NW width is proportional to the ratio between the surface energy and the elastic energy of the epilayer. It has been found that the surface energy is considerably influenced by the miscut angles.[21, 31, 41] The overall fact that the NW width is nearly not affected by

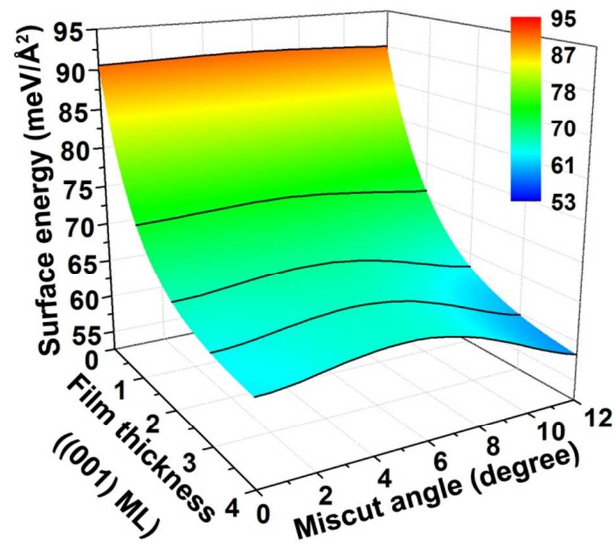

Figure 6 Graphical representation of the surface energy as a function of both the miscut angle and the thin film thickness. The latter in expressed in units of ML along the (001) direction. Solid lines show the surface energy at 0, 1, 2, 3, 4 (001) ML as a function of the miscut angle.

the miscut angle indicates that the variation in surface energy is balanced by that in elastic energy due to the anisotropicity of the vicinal surface. Our results disclose that the elastic energy on the vicinal surface is also considerably affected by the miscut angle. This finding is reasonable since both the surface energy and the elastic energy are associated with the steps on the vicinal surface, which depend on the miscut angle and azimuth particularly for thin epilayer. These are the main factors underlying the sensitive self-assembly of nanostructures on miscut substrates.[21, 41]

Next, we analyze the measurement of the wetting layers as a function of miscut angles. From a thermodynamic point of view, transition from a flat film to undulated surface occurs because elastic energy relaxation eventually overcomes the extra cost of creating an undulated surface during growth.[42] Recently, however, the surface energy as the dominant factor for the 2D to 3D transition has been pointed out for GeSi growth.[32, 43] This further justifies our choice of using *ab-initio* data for our surface energy function (Eq. (1)).[37] The WL thickness below the spontaneously formed NWs is,[34, 44]

$$h = -\omega_2 \delta \ln \frac{\omega_1 \delta^2}{4\kappa} \tag{3}$$

where $\omega_1 = \dfrac{2E_f\left(1-\nu_s^2\right)}{E_s\left(1-\nu_f\right)}$, $\omega_2 = \dfrac{1+\nu_f}{1-\nu_f} + \dfrac{E_f\left(1-2\nu_s\right)\left(1+\nu_s\right)}{E_s\left(1-\nu_f\right)}$,

with E_f, E_s, ν_f, ν_s being the Young's modulus and Poisson's ratio of the film and the substrate, respectively.[45] The variables $\kappa = \kappa(\theta)$ and $\delta = \delta(\theta)$ describe the functional form of γ as a function of thickness at a given miscut angle. In fact, Eq. (1) can be equivalently described as

$$\gamma(\theta, h) = \gamma_\infty(\theta)\left(1 + \kappa(\theta) e^{-\frac{h}{\delta(\theta)}}\right) \tag{4}$$

where $\gamma_\infty(\theta)$ is the thick-film limit value of the Ge surface energy. Both $\kappa(\theta)$ and $\delta(\theta)$, as well as $\gamma_\infty(\theta)$, are extracted numerically from the surface energy function in Eq. (1). By using Eq. 1 and the necessary constants for SiGe, we calculate the WL thickness as shown in Fig. 5 for the same indicative average alloy composition used before, namely 0.61, 0.66 and 0.71. Figures 4 and 5 show a very good agreement with the experimental measurements, confirming that a linear stability analysis approach is valid for early stages of thin-film growth. In particular, the calculations confirm that a minimum thickness is attainable for the vicinal substrates of around 6º. We explain this minimum by mainly considering the peculiar behavior of the surface energy as a function of miscut (Eq.1), as well as the strain energy. It is found that a maximum surface energy appears at around 6º miscut angle, as shown in Fig. 6. The higher energy of a vicinal surface results in the smaller cost of the surface energy due to surface undulation on the miscut substrate since the surface energies of (001) and {105} facets are essentially constant. In addition, based on the above discussion, the strain energy of the epilayer can also have a maximum value on the miscut substrate by an angle of ~6°, which facilitates the surface undulation for its relaxation. Both these two factors promote the early transition to the NW morphology because the elastic-energy relaxation provided by the surface undulations can readily overwhelm the cost of the surface energy. As a result of the interplay between surface and elastic energy, the critical thickness for NW formation on a vicinal surface is always smaller than for zero-degree miscut. In our view, this finding explains why the ripples are elongated along the [010] direction perpendicular to the miscut one. Along the [010] direction, the critical thickness for ripple formation will be the one at zero-degree miscut. Accordingly, the critical thickness for NW nucleation is always reached first along the miscut direction. Given that both the (105) and the (001) facets are the energetically favorable facets for the Ge-rich nanostructures, the readily available (105) and (001) facets on the miscut Si (001)/[100] θ (θ<11º) substrates result in the NWs perpendicular to the miscut directions. Whereas, on miscut Si (001) towards [110] direction substrates, the miscut angle θ dramatically limits the growth of long and fully-faceted NWs only to ~8º. In other words, NWs growth on [100] miscut has a much larger window of stable morphologies than on [110] miscut. Additionally, as it is well known, surface diffusion is strongly anisotropic across stepped surfaces.[45, 46]

The linear stability analysis approach based on ATG model has shown to correctly capture the early stage of thin film evolution.[29, 34, 44] Our results demonstrate that this method is valid also in the case of heteroepitaxial growth on the vicinal surface. In particular, at the early stage of growth, strain-driven surface roughening dominates over step-bunching growth instability.[47] In fact, kinetic or strain-driven step-bunching originates SiGe nanostructures with a base length ranging from 100 nm to more than 1μm, which is three to 50 times the size observed in our experiments.[25-28] However, we do not rule out the possibility that, by continuing SiGe deposition, the thin film morphology could be more strongly influenced by step bunching, eventually leading to a NW width comparable to the periodicity in the step bunches.

Our results clearly demonstrate that the vicinal surfaces offer an additional degree to control the growth behaviors of self-assembled NWs, particularly the height of NWs. Considering the smallest size with respect to the width and the length of the NWs, the height of NWs dominates the quantum confinement effect. As a result, it is a critical factor for the band gap, the oscillator strength and the spin-orbit interaction in NWs.[48] Meanwhile, the overall height variation along the direction perpendicular to laterally aligned NWs on the WL can also result in the transverse confinement of carriers due to the height-induced quantum confinement potentials. Unique transport properties in a single NW and anomalous magnetoresistance of the NW arrays have been discovered from these self-assembled GeSi NWs.[17, 49] Accordingly, the vicinal surfaces provides a direct way to tune the physical properties of NWs, as well as its growth. By optimizing the growth conditions, the miscut angle and even the patterning processes, the desired NWs with controlled size and arrangement are expected.[17, 50, 51] These laterally aligned and defect-free GeSi NWs can offer promising platforms to fully characterize the unique properties and explore the innovative device applications of NWs.

4. Conclusions

In summary, heteroepitaxial growth of Ge on the vicinal Si (001)/[100] θ (θ<11º) substrates shows the formation of the in-plane and catalyst-free GeSi NWs. All these self-assembled NWs laterally orient along the [010] direction. The NWs are rather stable and bounded by (001) and (105) facets. Moreover, by changing the miscut angle θ, the NW height can be easily modified, while the NW width is essentially not affected. Meanwhile, the thickness of the WL beneath the NWs varies with the miscut angle with a minimum at around 6º miscut. Our modeling study reveals the physical insights into the uniformity of the NW width and the peculiar behavior of the wetting layer thickness as a function of the miscut angle. It highlights the critical effects of the surface steps on both the surface energy and the strain energy of the epilayer on the vicinal surface, which dominate the self-assembly of nanostructures. Our results will promote the formation of desired NWs and other nanostructures on the vicinal surface since they can be intentionally modified by the miscut angle and the azimuth. Such self-assembled GeSi NWs on the vicinal surface are naturally aligned in-plane (without post-growth assembly), defect-free (without catalyst metal) and controllable, which will be the promising candidates for the full exploration of the unique properties and the innovative device applications of NWs.

Acknowledgement

T. Z. and G. V. contributed equally to the paper. This work was supported by the special funds for the Major State Basic Research Project (No. 2011CB925601) of China. G.V. and Y.-W. Z. gratefully aknowledge financial support from the Agency for Science, Technology and Research of Singapore (SERC Grants No. 132 550 4103 and 132 550 4106) as well as computing resources from A*STAR A*CRC.

Notes and references

[a] State Key Laboratory of Surface Physics and Department of Physics, Collaborative Innovation Center of Advanced Microstructures, Fudan University, Shanghai 200433, China
E-mail: zhenyangz@fudan.edu.cn
Fax: +86-21-65643278; Tel: +86-21-65643278
*[b] A*STAR Institute of High Performance Computing, 1 Fusionopolis Way #16-16, Connexis, Singapore 138632*
E-mail: vastolag@ihpc.a-star.edu.sg; zhangyw@ihpc.a-star.edu.sg

1. S. Nadj-Perge, S. M. Frolov, E. P. A. M. Bakkers and L. P. Kouwenhoven, *Nature*, 2010, **468**, 1084-1087.
2. S. M. Frolov, S. R. Plissard, S. Nadj-Perge, L. P. Kouwenhoven and E. P. Bakkers, *MRS Bull.*, 2013, **38**, 809-815.
3. C. Kloeffel, M. Trif and D. Loss, *Phys. Rev. B*, 2011, **84**, 195314.
4. J. Xiang, A. Vidan, M. Tinkham, R. M. Westervelt and C. M. Lieber, *Nat. Nanotechnol.*, 2006, **1**, 208-213.
5. B. Tian, X. Zheng, T. J. Kempa, Y. Fang, N. Yu, G. Yu, J. Huang and C. M. Lieber, *Nature*, 2007, **449**, 885-889.
6. N. P. Dasgupta, J. Sun, C. Liu, S. Brittman, S. C. Andrews, J. Lim, H. Gao, R. Yan and P. Yang, *Adv. Mater.*, 2014, **26**, 2137-2184.
7. P. Periwal, T. Baron, P. Gentile, B. Salem and F. Bassani, *APL Mater.*, 2014, **2**, 046105.
8. H. Adhikari, A. F. Marshall, C. E. D. Chidsey and P. C. McIntyre, *Nano Lett.*, 2006, **6**, 318-323.
9. Y. Li, R. Clady, J. Park, S. V. Thombare, T. W. Schmidt, M. L. Brongersma and P. C. McIntyre, *Nano Lett.*, 2014, **14**, 3427-3431.
10. R. S. Wagner and W. C. Ellis, *Appl. Phys. Lett.*, 1964, **4**, 89-90.
11. J. E. Allen, E. R. Hemesath, D. E. Perea, J. L. Lensch-Falk, Z. Y. Li, F. Yin, M. H. Gass, P. Wang, A. L. Bleloch, R. E. Palmer and L. J. Lauhon, *Nat. Nanotechnol.*, 2008, **3**, 168-173.
12. J. P. Colinge, C. W. Lee, A. Afzalian, N. D. Akhavan, R. Yan, I. Ferain, P. Razavi, B. O'Neill, A. Blake, M. White, A. M. Kelleher, B. McCarthy and R. Murphy, *Nat. Nanotechnol.*, 2010, **5**, 225-229.
13. J. Yao, H. Yan and C. M. Lieber, *Nat. Nanotechnol.*, 2013, **8**, 329-335.
14. M. Kwiat, S. Cohen, A. Pevzner and F. Patolsky, *Nano Today*, 2013, **8**, 677-694.
15. R. He, D. Gao, R. Fan, A. I. Hochbaum, C. Carraro, R. Maboudian and P. Yang, *Adv. Mater.*, 2005, **17**, 2098-2102.
16. S. T. Le, P. Jannaty, X. Luo, A. Zaslavsky, D. E. Perea, S. A. Dayeh and S. T. Picraux, *Nano Lett*, 2012, **12**, 5850-5855.
17. J. J. Zhang, G. Katsaros, F. Montalenti, D. Scopece, R. O. Rezaev, C. Mickel, B. Rellinghaus, L. Miglio, S. De Franceschi, A. Rastelli and O. G. Schmidt, *Phys. Rev. Lett.*, 2012, **109**, 085502.
18. P. D. Szkutnik, A. Sgarlata, A. Balzarotti, N. Motta, A. Ronda and I. Berbezier, *Phys. Rev. B*, 2007, **75**, 033305.
19. L. Persichetti, A. Sgarlata, M. Fanfoni and A. Balzarotti, *Phys. Rev. Lett.*, 2010, **104**, 036104.
20. G. Chen, B. Sanduijav, D. Matei, G. Springholz, D. Scopece, M. J. Beck, F. Montalenti and L. Miglio, *Phys. Rev. Lett.*, 2012, **108**, 055503.
21. T. Zhou and Z. Zhong, *APL Mater.*, 2014, **2**, 022108.
22. Y. W. Mo, D. Savage, B. Swartzentruber and M. Lagally, *Phys. Rev. Lett.*, 1990, **65**, 1020-1023.
23. M. R. McKay, J. Shumway and J. Drucker, *J. Appl. Phys.*, 2006, **99**, 094305.
24. M. Muhlberger, C. Schelling, G. Springholz and F. Schaffler, *Phys. E*, 2002, **13**, 990-994.
25. H. Lichtenberger, M. Mühlberger and F. Schäffler, *Appl. Phys. Lett.*, 2005, **86**, 131919.
26. F. Liu, J. Tersoff and M. G. Lagally, *Phys. Rev. Lett.*, 1998, **80**, 1268-1271.
27. V. Holy, A. A. Darhuber, J. Stangl, G. Bauer, J. Nutzel and G. Abstreiter, *Phys. Rev. B*, 1998, **57**, 12435-12442.
28. V. B. Shenoy and L. B. Freund, *J. Mechanics Physics Solids*, 2002, **50**, 1817-1841.

29. R. J. Asaro and W. A. Tiller, *Metall. Trans.*, 1972, **3**, 1789-1796.
30. D. J. Srolovitz, *Acta Metall.*, 1989, **37**, 621-625.
31. A. Ramasubramaniam and V. Shenoy, *J. Appl. Phys.*, 2004, **95**, 7813-7824.
32. M. Brehm, F. Montalenti, M. Grydlik, G. Vastola, H. Lichtenberger, N. Hrauda, M. J. Beck, T. Fromherz, F. Schäffler, L. Miglio and G. Bauer, *Phys. Rev. B*, 2009, **80**, 205321.
33. G.-H. Lu and F. Liu, *Phys. Rev. Lett.*, 2005, **94**, 176103.
34. J.-N. Aqua, T. Frisch and A. Verga, *Phys. Rev. B*, 2007, **76**, 165319.
35. L. Persichetti, A. Sgarlata, G. Mattoni, M. Fanfoni and A. Balzarotti, *Phys. Rev. B*, 2012, **85**, 195314.
36. J. N. Aqua, A. Gouye, A. Ronda, T. Frisch and I. Berbezier, *Phys. Rev. Lett.*, 2013, **110**, 096101.
37. D. Scopece, F. Montalenti and M. J. Beck, *Phys. Rev. B*, 2012, **85**, 085312.
38. T. Hammerschmidt, P. Kratzer and M. Scheffler, *Phys. Rev. B*, 2007, **75**, 235328.
39. J.-M. Zhang, Y. Zhang, K.-W. Xu and V. Ji, *Phys. B*, 2007, **390**, 106-111.
40. G. Vastola, V. B. Shenoy, J. Guo and Y. W. Zhang, *Phys. Rev. B*, 2011, **84**, 035432.
41. B. J. Spencer and J. Tersoff, *Appl. Phys. Lett.*, 2010, **96**, 073114.
42. G. Chen, E. Wintersberger, G. Vastola, H. Groiss, J. Stangl, W. Jantsch and F. Schäffler, *Appl. Phys. Lett.*, 2010, **96**, 103107.
43. J. Tersoff, B. Spencer, A. Rastelli and H. von Känel, *Phys. Rev. Lett.*, 2002, **89**, 196104.
44. J.-N. Aqua and T. Frisch, *Phys. Rev. B*, 2010, **82**, 085322.
45. J. Myslivecek, C. Schelling, F. Schaffler, G. Springholz, P. Smilauer, J. Krug and B. Voigtlander, *Surf. Sci.*, 2002, **520**, 193-206.
46. A. Pimpinelli, I. Elkinani, A. Karma, C. Misbah and J. Villain, *J. Phys.: Condens. Matter*, 1994, **6**, 2661-2680.
47. J. H. Zhu, K. Brunner, G. Abstreiter, O. Kienzle, F. Ernst and M. Ruhle, *Phys. Rev. B*, 1999, **60**, 10935-10940.
48. E. G. Barbagiovanni, D. J. Lockwood, P. J. Simpson and L. V. Goncharova, *Appl. Phys. Rev.*, 2014, **1**, 011302.
49. J. Z. Pan, T. Zhou, Z. M. Jiang and Z. Y. Zhong, *Appl. Phys. Lett.*, 2013, **102**, 183108.
50. H. Watzinger, M. Glaser, J. J. Zhang, I. Daruka and F. Schäffler, *APL Mater.*, 2014, **2**, 076102.
51. G. Chen, G. Springholz, W. Jantsch and F. Schäffler, *Appl. Phys. Lett.*, 2011, **99**, 043103.